

A Comparison of 2D and 3D Edge Detectors in Semi Automated Measurements of Chamber Volumes Using 3D Echocardiographic Laboratory Phantom Images

K Wang¹, AJ Sims^{1,2}, A Murray^{1,2}

¹Newcastle University, Newcastle upon Tyne, UK

²Regional Medical Physics Department, Freeman Hospital Newcastle Upon Tyne, UK

Abstract

Chamber volume measurement is fundamental for assessing many indices of cardiac function. 3D echocardiography offers great potential for accurate measurement, but many automated or semi-automated techniques suffer from acoustic noise and artefact, which can be reduced by suitable choice of edge detectors.

We compared the effects of 2D and 3D first order derivative edge detectors with similar size on accuracy and repeatability in six volume measurement methods of 3D echo images of a laboratory balloon phantom.

Overall accuracy compared with known volumes was better for 3D (-1.0ml; -4.0ml to 2.0ml 95% CI; P=0.53) than 2D (-11.6ml; -14.8ml to -8.5ml 95% CI; P<0.001). Repeatability was better for 3D (SD=0.9ml) than 2D (SD=1.5ml) with difference in coefficient of variation of 0.6 (P<0.001). 3D operators show potential for better performance with 3D echo images.

1. Introduction

Accurate, reproducible, noninvasive determination of cardiac chamber volume, especially left ventricular (LV) volume, is important for clinical assessment, risk stratification, selection of therapy, and serial monitoring of patients with cardiovascular disease [1-4]. In the last 15 years, developments in real time three-dimensional echocardiography (3DE) have achieved superior accuracy compared with conventional 2DE and performed comparably with radionuclide or magnetic resonance imaging (MRI) for measurement of cardiac ventricular volume [5, 6]. However, 3DE suffers from the limitations inherent to the ultrasonic imaging modality, including relatively poor spatial resolution, noise and artefact, which limit the accuracy and repeatability.

In automatic and semi-automatic measurement of chamber volume, suitable choice of edge detection operators can reduce the effects of noise. In this study, we aimed to compare the performance of 2D and 3D first order derivative edge detection operators in accuracy and

reproducibility of semi-automatic quantitative chamber volume measurements using a laboratory phantom.

2. Methods

2.1. Imaging acquisition

A Philips Sonos 7500 3D ultrasound system was used to image a balloon filled with water. The balloon was suspended in a water tank and imaged from above. Nine fill volumes (25ml, 50ml, 75ml, 100ml, 150ml, 200ml, 300ml, 400ml, 500ml) were scanned twice sequentially, which resulted in two 3D movies for each balloon volume. Each 3D movie consists of a sequence of 3D images (18-20 images). We measured volume for the first five 3D images from first movie of each balloon volume.

2.2. Image analysis

The two edge detection operators compared in this paper are 11×11 2D and $5 \times 5 \times 5$ 3D first order derivative Macleod operators [7]. The gradient operators were chosen to have similar size (121 pixels vs. 125 voxels) so that the number of neighbouring voxels which influence the result of applying an operator to a target voxel are similar.

Figure 1 shows examples of the effects of 2D and 3D edge detection operators. Figure 1 (a) is an original intensity image. After applying 2D and 3D gradient operators, two gradient images (b) and (c) respectively, were obtained.

To compare the performance of the two operators, we applied semi-automated quantitative techniques for chamber wall delineation and volume measurements. The long axis was defined manually by selecting one point near the apex and one point near the base of the balloon. After this manual initialization, the wall detection algorithm searched for the segments of the inner wall in a series of contiguous short axis planes perpendicular to the long axis, from the apex to the base. Balloon volumes were calculated by integration of the detected boundary

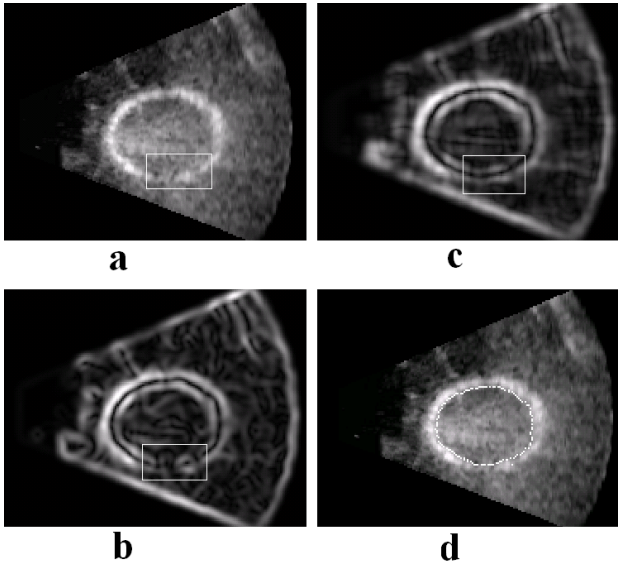


Figure 1. Effects of 2D and 3D edge detection operators and the wall delineation result of G2B1I2. (a): a 2D short axis slice extracted from a 3D image; (b): gradient image obtained by using 11×11 Macleod operator; (c): gradient image obtained by using $5 \times 5 \times 5$ Macleod operator. (d): after applying G2+B1+I2, the detected inner wall boundary are shown in white

area of all short axis planes. Due to the noise and artefacts, the wall detection algorithm cannot detect all the wall segments, and an interpolation algorithm was used to interpolate these missing segments. The whole process of this semi-automated volume measurement technique is illustrated in Figure 2.

We used a capital letter and a number to code every algorithm, as shown in Figure 2. B1 detects the inner wall edges based only on the gradient image and B2 combines the intensity information of original and gradient images together to detect the edges. I1 interpolates missing segments linearly and I2 uses an elliptic fit. For each gradient operator, G1 or G2, there are six different combinations (six methods) for delineating the chamber wall boundary, which are: B1, B2, B1I1, B2I1, B1I2 and B2I2. Figure 1 (d) gives an example of chamber wall delineation starting with B1I2 in figure legend.

2.3. Measurement and comparison

In total, 540 measurements of volume (two operators \times six methods \times nine balloon volumes \times five 3D images) were obtained. All comparisons were expressed as bias \pm SD.

We applied the method of Bland and Altman [8] to assess the accuracy of G1 and G2 by comparing the measured volume using G1 (V_{G1}) with known volume

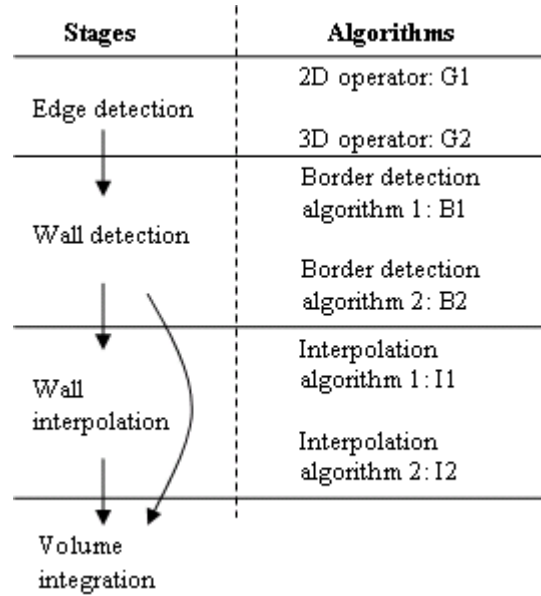


Figure 2. Flowchart of the volume calculation procedure

(V_K) and measured volume using G2 (V_{G2}) with V_K in actual value (ml). We also compared V_{G1} with V_{G2} in both actual volume (ml) and relative value (measured volume/ V_K , %).

To evaluate the reproducibility of G1 and G2, the standard deviation (SD) and coefficient of variation (CV) of every five measurements of five images for each delineation method and balloon volume were calculated (54 SD and 54 CV). Student t test was applied to compare the CV between V_{G1} and V_{G2} , and an ANOVA was used to compare the mean and differences of SD.

3. Results

For accuracy, results of comparisons of V_{G1} , V_{G2} with V_K , and V_{G1} with V_{G2} are given in Table 1. An example of Bland-Altman plots for method B1I1 and B2I2 is shown in Figure 3 (a). For G1, we found one method (B1I1) that showed no statistically significant difference with V_K ($P=0.22$). For G2, two methods (B2I1 and B2I2) showed no significant differences ($P=0.12$ and 0.09). For all six methods together, significant difference with V_K was detected for G1 ($P<0.001$), but was not detected for G2 ($P=0.53$). This is also illustrated in Figure 3 (b), which shows two comparisons of V_{G1} , V_{G2} with V_K , respectively, in all six methods ($n = 270$ in each case). We found significant difference between V_{G1} and V_K (bias=-11.6ml; -14.8ml to -8.5ml 95% CI), but not for V_{G2} (bias=-1.0ml; -4.0ml to 2.0ml 95% CI).

For $V_{G2}-V_{G1}$, we found positive bias for all six methods (last two columns of Table 1). The differences were significant for every method ($P<0.001$ in ml and %),

Table 1. For accuracy, the summary of Bland-Altman comparisons (bias \pm SD) of V_{G1} , V_{G2} with V_K respectively, and V_{G1} with V_{G2} for six chamber wall delineation methods (n=45 in each method)

| Method | 2D- | 3D- | 3D-2D | (3D-2D) % |
|-------------|---|---|-------------|--------------|
| | known volume $V_{G1}-V_K$ (ml) | known volume $V_{G2}-V_K$ (ml) | | |
| B1 | -27 \pm 26 | -17 \pm 20 | 9 \pm 9 | 5 \pm 3 |
| B2 | -38 \pm 31 | -26 \pm 17 | 13 \pm 15 | 5 \pm 4 |
| B1I1 | 3 \pm 17* | 12 \pm 21 | 9 \pm 10 | 4 \pm 2 |
| B2I1 | -8 \pm 12 | 4 \pm 16* | 12 \pm 13 | 4 \pm 3 |
| B1I2 | 7 \pm 22 | 16 \pm 27 | 10 \pm 10 | 4 \pm 2 |
| B2I2 | -7 \pm 14 | 5 \pm 20* | 12 \pm 13 | 5 \pm 3 |
| All methods | -12 \pm 21 | -1 \pm 20* | 11 \pm 12 | 5 \pm 3 |
| P Value | <0.001 | 0.53* | <0.001 | <0.001 |

Note: * no significant difference detected

as shown in Figure 4 (the 95% confidence intervals of all six methods do not include zero). Typically, volumes calculated using G2 are about 5% larger than those calculated using G1.

Table 2. For repeatability, the summary of comparisons (bias \pm SD) of coefficient of variation (CV) between G1 and G2 for six methods (n=9 in each method)

| Method | Coefficient of variation |
|-----------------|--------------------------|
| | 2D-3D |
| B1 | 0.6 \pm 0.9 |
| B2 | 1.1 \pm 1.4 |
| B1I1 | 0.6 \pm 0.6 |
| B2I1 | 0.5 \pm 0.7 |
| B1I2 | 0.3 \pm 1.0 |
| B2I2 | 0.2 \pm 1.0 |
| All six methods | 0.6 \pm 1.0 |
| Probability | <0.001 |

For repeatability, Table 2 shows the comparisons of CV between G1 and G2. For every chamber wall delineation method, the CV of G1 is larger than G2. Paired student t test showed that the difference was significant (P<0.001). The ANOVA of SD also indicated that there were significant differences between G1 and G2 (F=11.0; P=0.001; G1: mean SD=1.5 ml; G2: mean SD = 0.9 ml). These results tell us that the coefficient of variation and the standard deviation of G2 are significantly smaller than G1; the reproducibility of G2 is better.

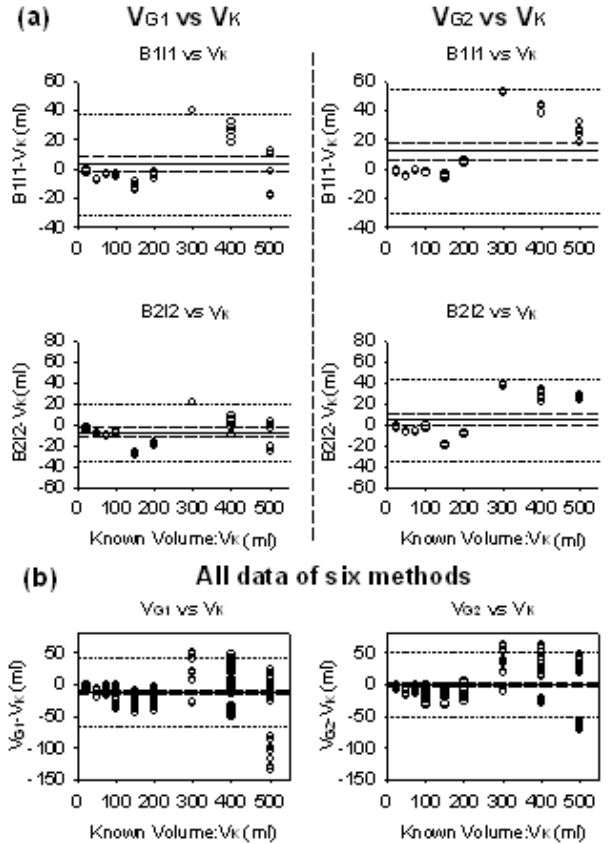


Figure 3. Bland-Altman plots: (a) comparison of V_{G1} , V_{G2} with V_K in ml for volume measurement method B1I1 and B2I2. (b) comparison of V_{G1} , V_{G2} with V_K in ml respectively. Solid lines: bias (mean); dash lines: 95% confidence interval (CI) of bias; dotted lines: upper and lower limits of agreement

4. Discussion and conclusions

For ultrasound images, the signal to noise ratio is often poor, and acoustic noise can confound the detection of cardiac chamber wall boundary. After applying edge detection operators, this problem can be partially alleviated by extending the size of the neighbourhoods over which the differential gradients are computed [7], but the apparent width of the edges (wall boundaries) will be broadened as a consequence. There is a trade-off between noise reduction and resolving power.

With 3D edge detections, the addition of z direction for the operator can gather extra information from the neighbourhood whilst keeping the size in all directions relatively small. For this reason, the 3D operator can sometimes limit the artifacts and noise effects on the ultrasound images. Figure 1 (a) and (b) shows that a small part of the balloon wall is missed using a 2D

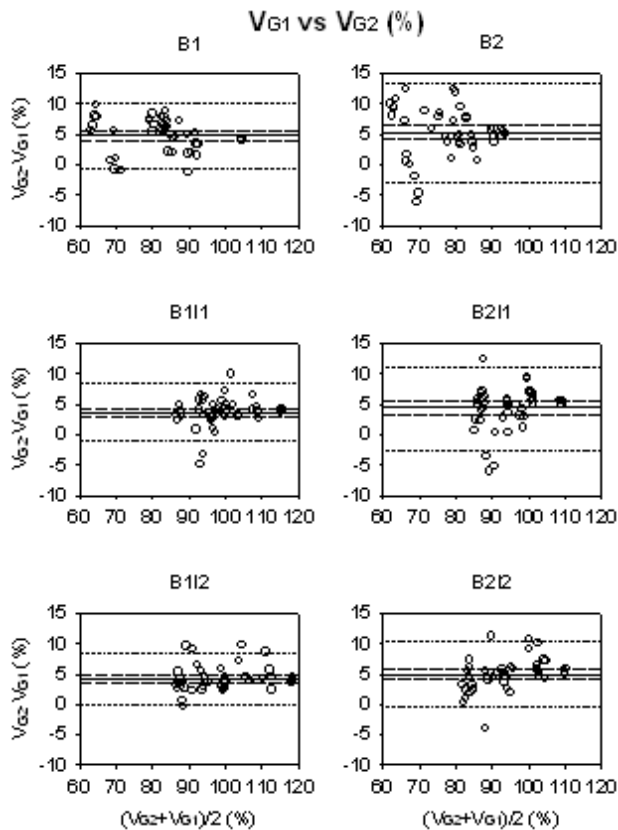


Figure 4. Bland-Altman plots comparing V_{G1} with V_{G2} in relative values (%) for six volume measurement methods. Solid lines: bias (mean); dash lines: 95% confidence interval of bias; dotted lines: upper and lower limits of agreement

operator (highlighted area). This gap is restored in (c) because of the action of 3D operators.

In this research, we found that for the similar size of two operators (121 pixels vs. 125 pixels), the measured volume of six semi-automated methods together after applying 3D gradient operator showed no statistically significant difference with known volume, whereas after applying 2D operator, the results showed significant difference.

For repeatability, we found that the coefficient of variation and the standard deviation of data measured by 2D operator are significantly larger than data measured by 3D.

We conclude that comparing with a 2D first order differential gradient operator, a 3D operator can improve the accuracy as well as the reproducibility of quantitative volume measurement in real time 3D echocardiographic images, when both gradient operators contain similar number of pixels.

Acknowledgements

We thank Joanne Wild and James Pemberton for their help with collection of the balloon images.

References

- [1] Rogers WJ, Canto JG, Lambrew CT. Temporal trends in the treatment of over 1.5 million patients with myocardial infarction in the U.S. from 1990 through 1999: the national registry of myocardial infarction 1, 2 and 3. *J Am Coll Cardiol* 2000; 36: 2056-63.
- [2] White HD, Norris RM, Brown MA, Brandt PW, Whitlock RM, Wild CJ. Left ventricular end-systolic volume as the major determinant of survival after recovery from myocardial infarction. *Circulation* 1987; 76: 44-51.
- [3] Krumholz HM, Chen YT, Wang Y, Vaccarino V, Radford MJ, Horwitz RI. Predictors of readmission among elderly survivors of admission with heart failure. *Am Heart J* 2000; 139: 72-7.
- [4] Kirkpatrick JN, Vannan MA, Narula J, Lang RM. Echocardiography in Heart failure: applications, utility, and new horizons. *J Am Coll Cardiol* 2007; 50: 381-96.
- [5] Gopal AS, Keller AM, Rigling R, King DL Jr, King DL. Left ventricular volume and endocardial surface area by three-dimensional echocardiography: comparison with two-dimensional echocardiography and nuclear magnetic resonance imaging in normal subjects. *J Am Coll Cardiol* 1993; 22: 258-70.
- [6] Nosir YFM, Fioretti PM, Vletter WB, Boersma E, Salustri A, Postma JT, Reijts AEM, Ten Cate FJ, Roelandt JRTC. Accurate measurement of left ventricular ejection fraction by three-dimensional echocardiography. A comparison with radionuclide angiography. *Circulation* 1996; 94: 460-6.
- [7] Pratt WK. Digital image processing, second edition. John Wiley & Sons, USA 1991.
- [8] Bland J, Altman D. Statistical methods for assessing agreement between two methods of clinical measurement. *Lancet* 1986; 1:307-310.

Address for correspondence

Kun Wang
Newcastle University
Newcastle upon Tyne
NE1 7RU
UK

Kun.Wang@ncl.ac.uk